2.3 Far offset data processing IPP's

In this section, the far offset processing will be reviewed and case studies showing the use of interpretive processing within far offset processing will be illustrated. The "normal" far offset processing will consist of

(1) polarization of the **X(FRT)** and **Y(FRT)** data into **HMAX(FRT)** and **HMIN(FRT)** data: the **HMAX(FRT)** data is the projection of the **X(FRT)** and **Y(FRT)** data into a plane defined by the well and the source location;

(2) polarization of the **HMAX(FRT)** and **Z(FRT)** data into **HMAX'(FRT)** and **Z'(FRT)** data: the **HMAX'(FRT)** data will be polarized in the direction of source and the **Z'(FRT)** data will be orthogonally polarized to **HMAX'(FRT)**;

(3) wavefield separation of the **Z'(FRT)** and **HMAX'(FRT)** data into $\mathbf{Z'_{up}(FRT)}$ and $\mathbf{HMAX'_{up}(FRT)}$ data;

(4) wavefield separation of the **HMAX'(FRT)** data into $\mathbf{HMAX'_{down}(FRT)}$ data: this will be used to deconvolve the final output, $\mathbf{Z''_{up}(FRT)}$ into $\mathbf{Z''_{up(decon)}(FRT)}$;

(5) derotation (Hinds et al., 1989a) of the $\mathbf{Z'_{up}(FRT)}$ and **HMAX'(FRT)** data into $\mathbf{Z_{up(derot)}(FRT)}$ and $\mathbf{HMAX_{up(derot)}(FRT)}$ data;

(6) time-variant polarization of the $\mathbf{Z_{up(derot)}(FRT)}$ and $\mathbf{HMAX_{up(derot)}(FRT)}$ data into

Z"$_{up}$(FRT) and **HMAX"$_{up}$(FRT)** data;

(7) VSP-CDP or migration of the **Z"$_{up}$(+TT)** data into the **+TT** versus offset from the well domain.

In the interpretation of the far offset IPP's, a number of crucial observations are being made. Some of the questions are:

(1) do the **X**, **Y**, and **Z** data obey the assumptions behind the time invariant polarizations reviewed in chapter 1 (section 1.4.3) ?
(2) what are the origins of noise seen on the data ?
(3) how is the noise being propagated onto the output data panels following each processing stage ?
(4) what is the multiple event content in the VSP-CDP or migrated data ?
(5) do the multiples in the VSP-CDP or migrated data interfere with the interpretation of primary events ?
(6) Can the primary and multiple events be differentiated since reflectors imaged away from the well may not intersect the first break curve ?

These questions will be posed again and again during the interpretive processing of the far offset IPP's. The partitioning of the energy of the various wavefields onto the polarization axis and time-variant "axis" will be illustrated using the far offset data contained in Chapter 4 (Ricinus carbonate reef case study; Hinds et al., 1989a; Hinds et al., 1993c; Hinds et al.,

1994c), Chapter 5 (Fort St. John Graben case study; Hinds et al., 1991a; Hinds et al., 1993a and 1994b; Hinds et al. 1994b) and Chapter 6 (Simonette carbonate reef case study; Hinds et al., 1991b; Hinds et al., 1993b and 1994c). The success and failures of far offset deconvolutions will be illustrated using Chapter 4 and 6 data.

A review of the Ricinus carbonate reef case study polarization IPP's will show:

(1) the results after using "normal" processing runstreams (see section 2.1);

(2) an analysis of the noise on the polarized results; and

(3) the modification of the processing runstream to enhance the interpretation of the $\mathbf{Z''_{up}(+TT)}$ data.

2.3.1 Time invariant polarization: isolation of the downgoing P-wave

In this section, the **Z(FRT)**, **X(FRT)** and **Y(FRT)** data are polarized to isolate the downgoing P-wave events onto a single data panel, **HMAX'(FRT)**. The orthogonal data projection, **Z'(FRT)**, was considered in the past to contain predominantly upgoing P-wave events. Interpretation would be performed on the wavefield separated $\mathbf{Z'_{up}(+TT)}$ data and on the VSP-CDP transformed upgoing events. In the next section, time variant polarization will be used to isolate the upgoing P-wave events onto a single output panel, $\mathbf{Z''_{up}(+TT)}$.

The polarization analysis presented in this section use hodogram derived rotation angles derived in a time invariant sense. The hodogram analysis is performed on a single window of data around the first breaks of the two input VSP data to yield a single polarization angle.

In the next section, the polarization angle for a pair of input traces is allowed to vary in time along the traces.

In Figure 2.41, the time invariant polarization IPP for the far offset data (700 m offset source location; source location in a direction of 307° from the well) of the Fort St. John Graben case study (Chapter 5) is shown. For reference within this chapter and chapter 5, the dataset will be referred to as the FSJG1 data.

The **X(FRT)**, **Y(FRT)**, and **Z(FRT)** data are shown in panels 1, 2, and 3, respectively. The downgoing P-wave events in the **Z(FRT)** data of panel 3 are highlighted in yellow. In comparison to the panels 1 and 2, the **Z(FRT)** data contain the majority of the downgoing P-wave events.

Primary downgoing P-wave energy is divided in varying amounts on the **X(FRT)** and **Y(FRT)** data shown in panels 1 and 2 (highlighted in yellow) indicating that the geophone sonde was rotating within the borehole during the acquisition of the data. However, the first break wavelet on the two panels show the most consistency for the bottom two-thirds of the borehole indicating that the sonde was rotating slowly during the acquisition at those depths.

The **Z(FRT)** data shown in panel 3 contains a diffraction event (highlighted in purple) in the lower left hand corner of the panel. This diffraction will be unfortunately partitioned onto all of the output data panels (see highlighted purple events in panels 5-7) as a result of further processing. Since these diffraction events are not polarizable in the same way that the up-

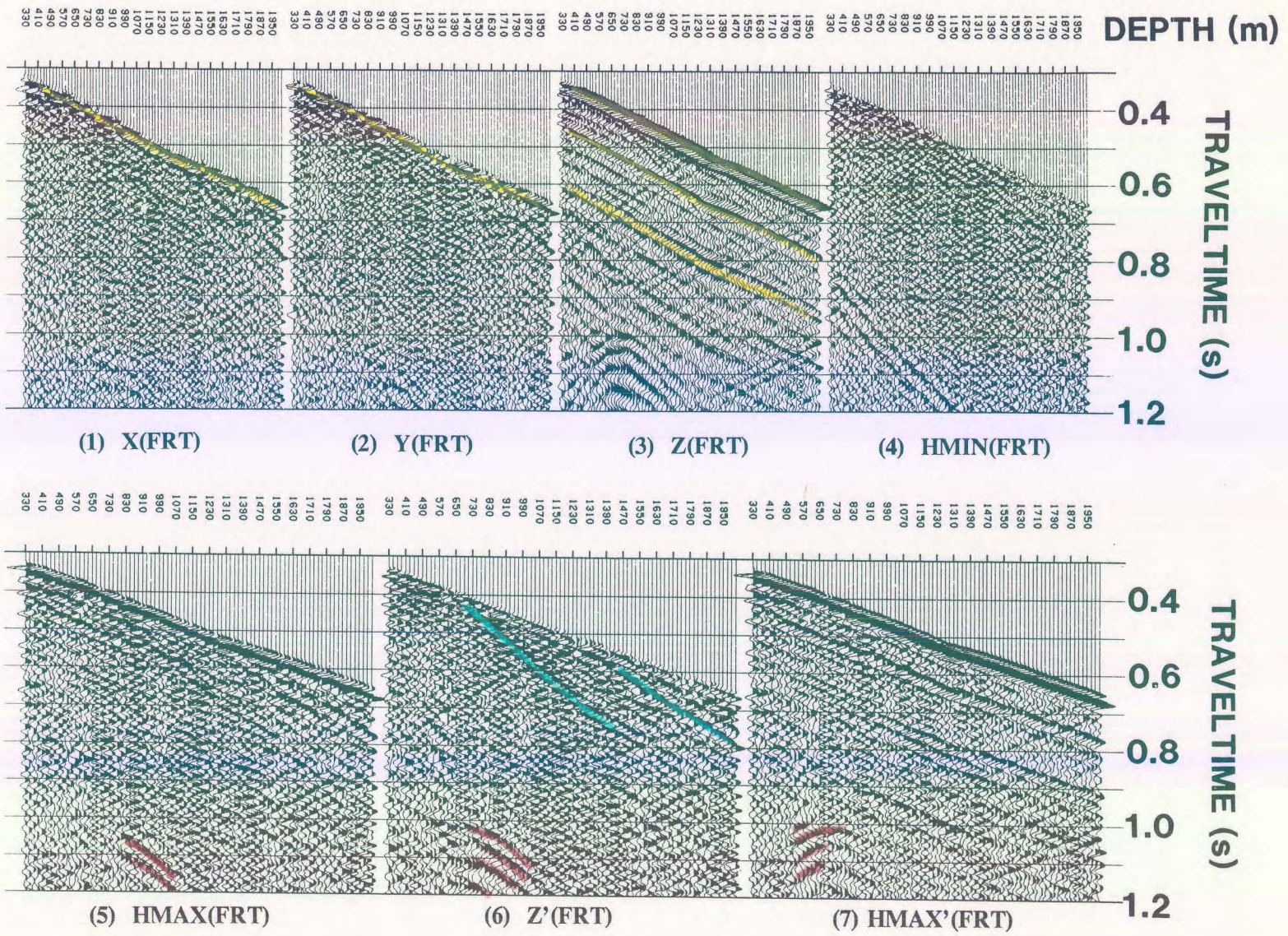

Figure 2.41 Hodogram-based polarization IPP for the Fort St. John Graben (FSJG1) far offset data (Hinds et al., 1993a). The downgoing P-wave events have been isolated on the **HMAX'(FRT)** data in panel (7).

and downgoing P-wave events are, interpretation will be performed "over" these "noise" events.

The result of hodogram based polarization analysis on the **X(FRT)** and **Y(FRT)** data and subsequent "single angle" rotation yields the **HMIN(FRT)** and **HMAX(FRT)** data shown in panels 4 and 5, respectively. The minor amount of downgoing P-wave events evident in the **X(FRT)** and **Y(FRT)** data shown in panels 1 and 2 have been isolated within the **HMAX(FRT)** data of panel 5.

The rotation of the **X(FRT)** and **Y(FRT)** data was performed using an interactive hodogram analysis program. A window of input data, from the **X(FRT)** and **Y(FRT)** data, centred around the first break of two input traces at the same depth recording level are shown in one portion of the screen. The trace data are colour coded so that hodogram points shown in another portion of the screen can be correlated to the traveltime of the trace data. This enables an interpretation of the hodogram plot. A least squares routine estimates the best straight line through the cloud of hodogram points. The **HMAX(FRT)** and **HMIN(FRT)** windowed results using the rotation angle determined by the least-squares fit is displayed onto another portion of the monitor. The user can now interactively alter the angle of the straight line through the hodogram cloud of points and the displayed window of **HMAX(FRT)** and **HMIN(FRT)** output traces (also centred around the first break) immediately change according to the updated rotation angle. The calculations which produce the **HMIN(FRT)** and **HMAX(FRT)** traces use the rotation matrix shown in the Appendix.

During the determination of the rotation angle using the hodogram plot and the various

screen displays, the aim is to:

(1) to maximize the amount of downgoing P-wave first break energy on the **HMAX** trace; and

(2) produce a consistent output polarity.

The polarity of the **HMAX(FRT)** data in panel 5 is consistent and minimal downgoing P-wave energy can be seen on the **HMIN(FRT)** data in panel 4. Mode-converted downgoing SV events are highlighted (in blue) on the **HMAX(FRT)** in panel 5.

The **Z'(FRT)** and **HMAX'(FRT)** data calculated using a hodogram analysis and subsequent rotation of the **HMAX(FRT)** and **Z(FRT)** data are shown in panels 6 and 7, respectively. The downgoing P-wave data are isolated onto the **HMAX'(FRT)** panel and the **Z'(FRT)** data contains mode-converted SV energy (highlighted in blue). Mode-converted SV downgoing events on the **Z'(FRT)** data appear to originate at the impedance boundaries at 690 m (Spirit River Formation; see Chapter 5) and the 1260 m (Nordegg Formation; see Chapter 5). Upgoing P events can be identified on panel 6 from the Nordegg reflector (highlighted in orange).

The diffraction event seen clearly on the **Z(FRT)** data has now been partitioned onto both the **HMAX'(FRT)** and **Z'(FRT)** data. Interestingly enough, the **HMAX'(FRT)** data contain the "upgoing" part of the diffraction and the **Z'(FRT)** data contain the "downgoing" part of the event.

2.3.2 Time variant polarization: isolation of the upgoing P-wave events

In this section, time variant polarization will be applied to the upgoing events from the **HMAX'$_{up}$(FRT)** and **Z'$_{up}$(FRT)** data to yield the **Z"$_{up}$(FRT)** data. The final interpretations are done on the **Z"$_{up}$(+TT)** and the VSP-CDP transformed and/or migrated **Z"$_{up}$(+TT)** data.

The time invariant polarizations performed in the previous section assumed that a single angle was adequate to polarize the up- and downgoing **Z(FRT)** and **HMAX(FRT)** event onto separate panels, **Z'(FRT)** and **HMAX'(FRT)**. The polarization angle needed to isolate (polarize) the upgoing P-wave onto the **Z"$_{up}$(FRT)** data is time variant. The angle of reflection from interfaces below the sonde change with depth as is shown in Figure 2.42. This implies that the incident angle of the upgoing P-wave events at a single geophone location changes accordingly with recording time.

The **Z'$_{up}$(FRT)** and **HMAX'$_{up}$(FRT)** data are a result of performing wavefield separation on the **Z'(FRT)** and **HMAX'(FRT)** data, respectively. The IPP for the time variant polarization of the FSJG1 far offset data is shown in Figure 2.43. The **Z'$_{up}$(FRT)** and **HMAX'$_{up}$(FRT)** data shown in panels 1 and 2, respectively, contain:

(1) upgoing P events (highlighted in orange);

(2) possible diffraction appear between 0.4 - 0.6 s (highlighted in brown); and

(3) mode converted downgoing shear wave events (highlighted in blue).

The **Z$_{up(derot)}$(FRT)** and **HMAX$_{up(derot)}$(FRT)** data shown in panels 3 and 4 are formed from **Z'$_{up}$(FRT)** and **HMAX'$_{up}$(FRT)** data by applying a rotation operation opposite to that used

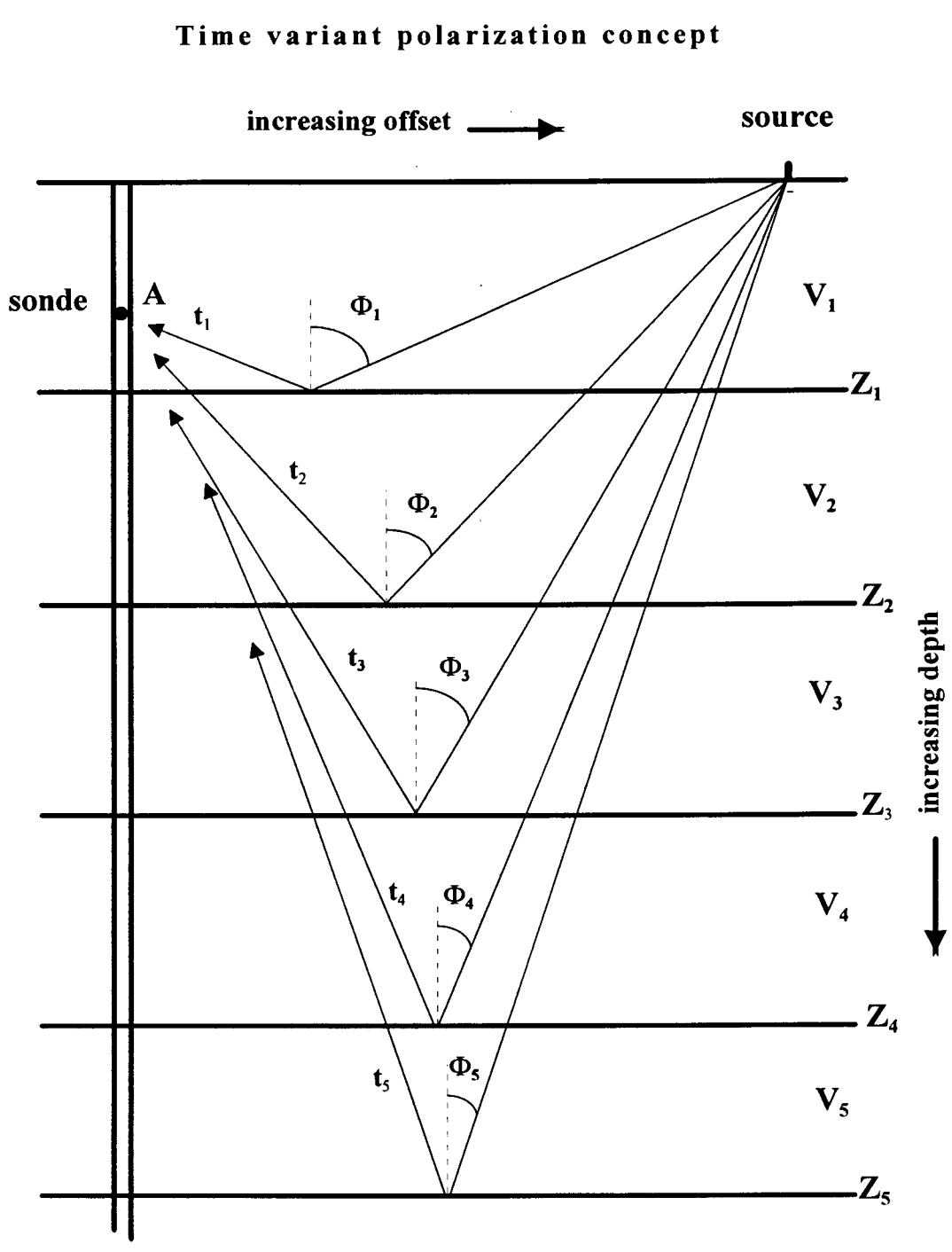

Figure 2.42 The reflection angle for upgoing raypaths emerging at the geophone at A from deeper interfaces decreases in comparison to the reflections from shallower interfaces. The Φ_i are the reflection angles, V_i are the layer velocities, Z_i are the layer depths and t_i are the raypath traveltimes to the sonde at **A.**

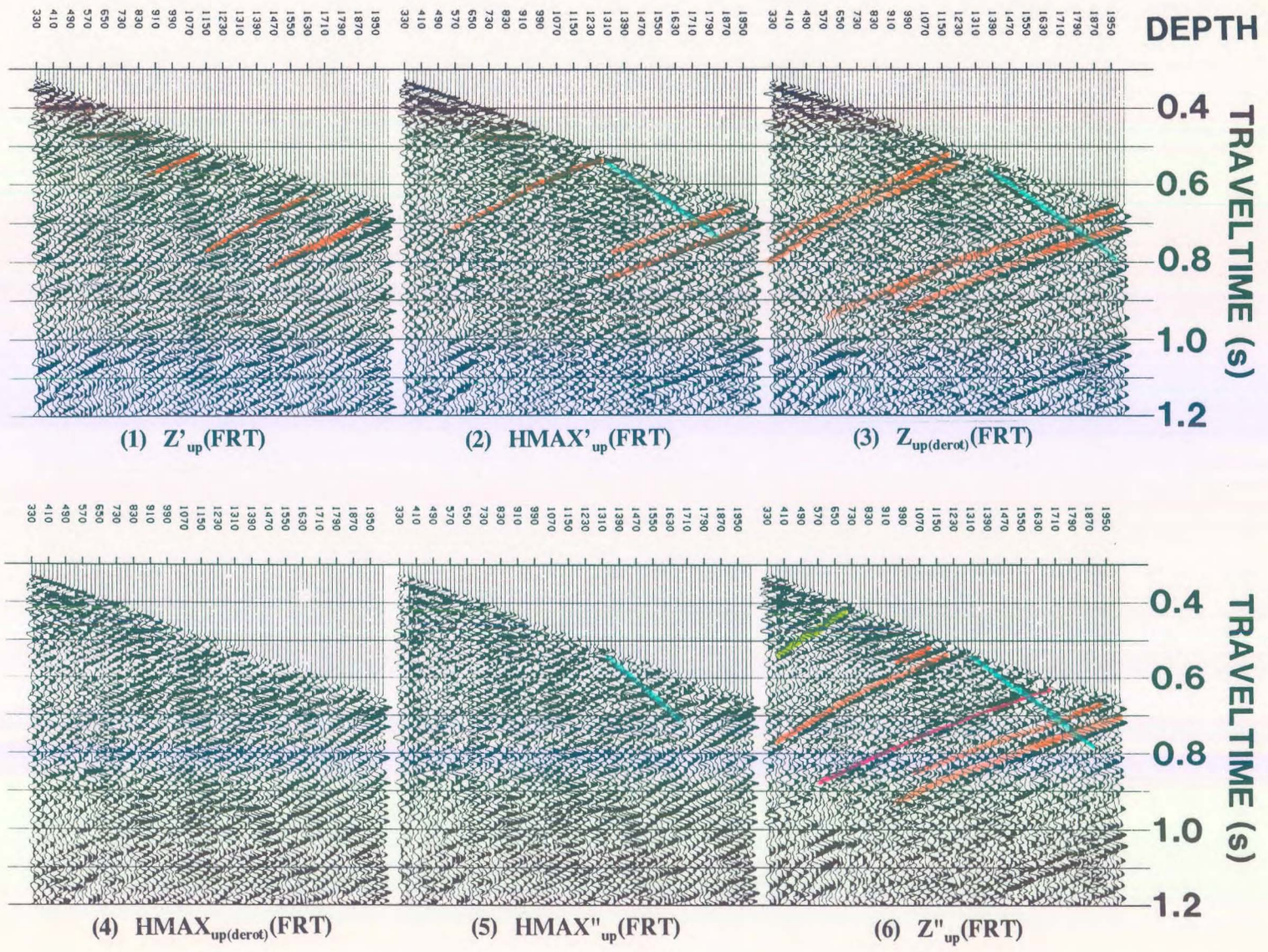

Figure 2.43 Time-variant polarization IPP for the Fort St. John Graben (FSJG1) far offset data (Hinds et al., 1993a). The upgoing P-wave events have been predominately partitioned onto the **Z"$_{up}$(FRT)** panel.

in calculating the **Z'(FRT)** and **HMAX'(FRT)** data. By inspection of panels 3 and 4, it appears as if this simple derotation is already isolating the upgoing P-wave events (highlighted in orange in panel 3).

The interval velocities and first break times from the near offset VSP data of the Fort St. John Graben case study are used to construct a model for ray-tracing. The first breaks (when the downgoing P-wave should reach an interface) and the velocity of the various interfaces (which will be used to propagate the upgoing reflections) are derived through simple calculations. The ray-tracing to the defined geophone locations (given the source offsets) will result in the (time,angle) pairs to be used in time-variant polarization (see Appendix). The result of the time-variant polarization is **HMAX"$_{up}$(FRT)** and **Z"$_{up}$(FRT)** shown in panels 5 and 6 (Fig. 2.43), respectively.

By inspection of panels 3 and 6 ($\mathbf{Z_{up(derot)}}$ and **Z"$_{up}$**), the downgoing (residual) SV events seen on panel 3 are now mapped jointly onto panel 5 and 6 (coloured in blue). The upgoing P event (coloured pink) originating near the 1750 m depth is more interpretable on the **Z"$_{up}$(FRT)** data in panel 6. The shallow Spirit River event (coloured green on panel 6) at 690 m which was not resolved on panels 1 to 4 can now be interpreted. Other upgoing events on the **Z"$_{up}$(FRT)** data have been coloured orange in panel 6.

2.3.3 VSP-CDP Transformation and Migration

In this section, the $\mathbf{Z''_{up}(FRT)}$ data are VSP-CDP transformed or migrated and the IPP designed to utilize interpretive processing is presented. The term VSP-CDP or "VSP-CDP mapping" refers to mapping the VSP data into a pseudoseismic section that displays coverage starting from the borehole out to the furthest reflection defined by the VSP data geometry and input velocity model (Wyatt and Wyatt, 1981; Millahn et al., 1983). The product of the VSP-CDP mapping has been called the VSPCDP (Hardage, 1985). The VSP-CDP and migration far-offset IPP for the FSJG1 data (chapter 5) is shown in Figure 2.44.

The $\mathbf{Z''_{up}(+TT)}$ and $\mathbf{Z''_{up(med)}(+TT)}$ data are shown in panels 1 and 2, respectively. The VSP-CDP (Dillon and Thomson, 1984) mapped $\mathbf{Z''_{up}(+TT)}$ data are shown in panel 3. Note that the horizontal axis for panel 3 (and 4) is not depth but offset distance from the well. The image of the reflectors on the VSP-CDP or migrated data is similar to how the reflectors would appear on a seismic section.

The IPP is completed with a Kirchhoff migrated version of the $\mathbf{Z''_{up}(+TT)}$ data shown in panel 4. The migrated data appear to be "smoother" than the VSP-CDP mapped data of panel 3. The events between 1.2 and 1.35 s display faulting. An example of the faulting is highlighted by the event in green and interpreted faults (in pink) on panels 3 and 4.

One of the most important interpreted events is a dominant peak (in blue) at 1.27 s which exists laterally from the well out to a distance of 55 to 75 m away from the well. The amplitude of the event attenuates rapidly at offsets beyond that point and may represent a

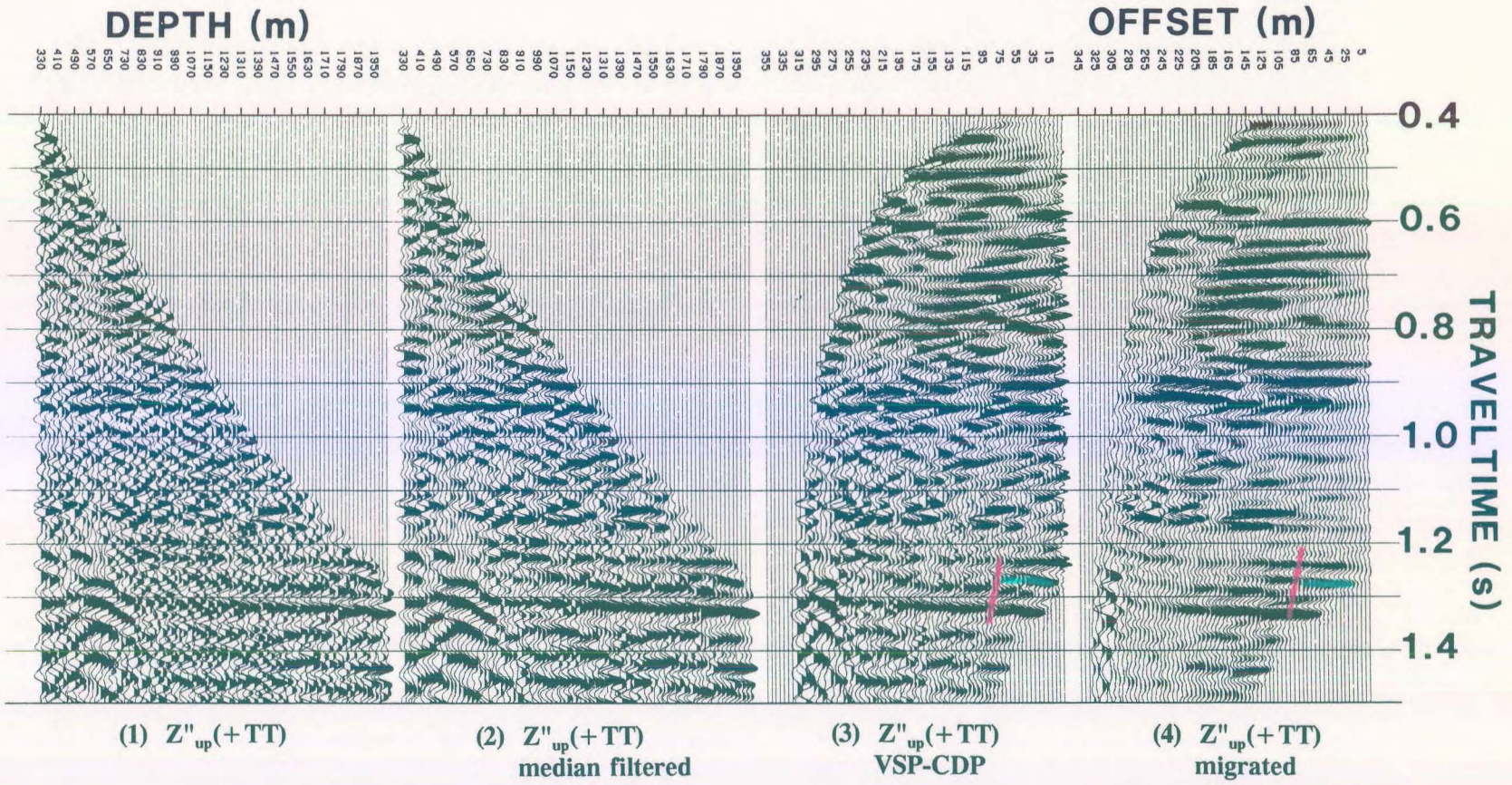

Figure 2.44 VSP-CDP and Kirchhoff migration IPP for the Fort St. John Graben (FSJG1) far offset data (Hinds et al., 1993a). Note the termination of the event (peak) on the VSP-CDP at 1.27 s (panels 3 and 4). The event exists only on offset traces 0-55 m.

possible facies change in the basal Kiskatinaw (chapter 5 and in Hinds et al., 1991a; Hinds et al., 1993a and 1994b; Hinds et al., 1994c). This observation is an important consideration for exploration. Beyond the interpreted fault (in pink) at a distance of 95 to 115 m offset from the well, the event appears to terminate.

The other far offset data for the Fort St. John Graben case study (source location offset of 741 m; location of offset source is East of the well) will be referred to as the FSJG2 data. Figures 2.45, 2.46, and 2.47 display the far-offset IPP's for the FSJG2 data.

By following the rotation processes on these figures, it can be interpreted that the event at 1.25 - 1.27 s on the VSPCDP and migrated $\mathbf{Z''_{up}(+TT)}$ data (coloured blue) in panels 3 and 4 of Figure 2.47 does not terminate near the well. The event is laterally more continuous than the same event on the FSJG1 data seen in panels 3 and 4 of Figure 2.44. Faulting (shown in pink) is also evident on the VSPCDP and migrated data in Figure 2.47 between 1.1 and 1.35 s.

2.3.4 Far offset deconvolution

In this section, the deconvolution of the far offset VSP data is reviewed and far offset deconvolution IPP's are presented. The process of far offset deconvolution is the spectral division of the $\mathbf{Z''_{up}(FRT)}$ data by the $\mathbf{HMAX'_{down}(FRT)}$ data to output the $\mathbf{Z''_{up(decon)}(FRT)}$ data.

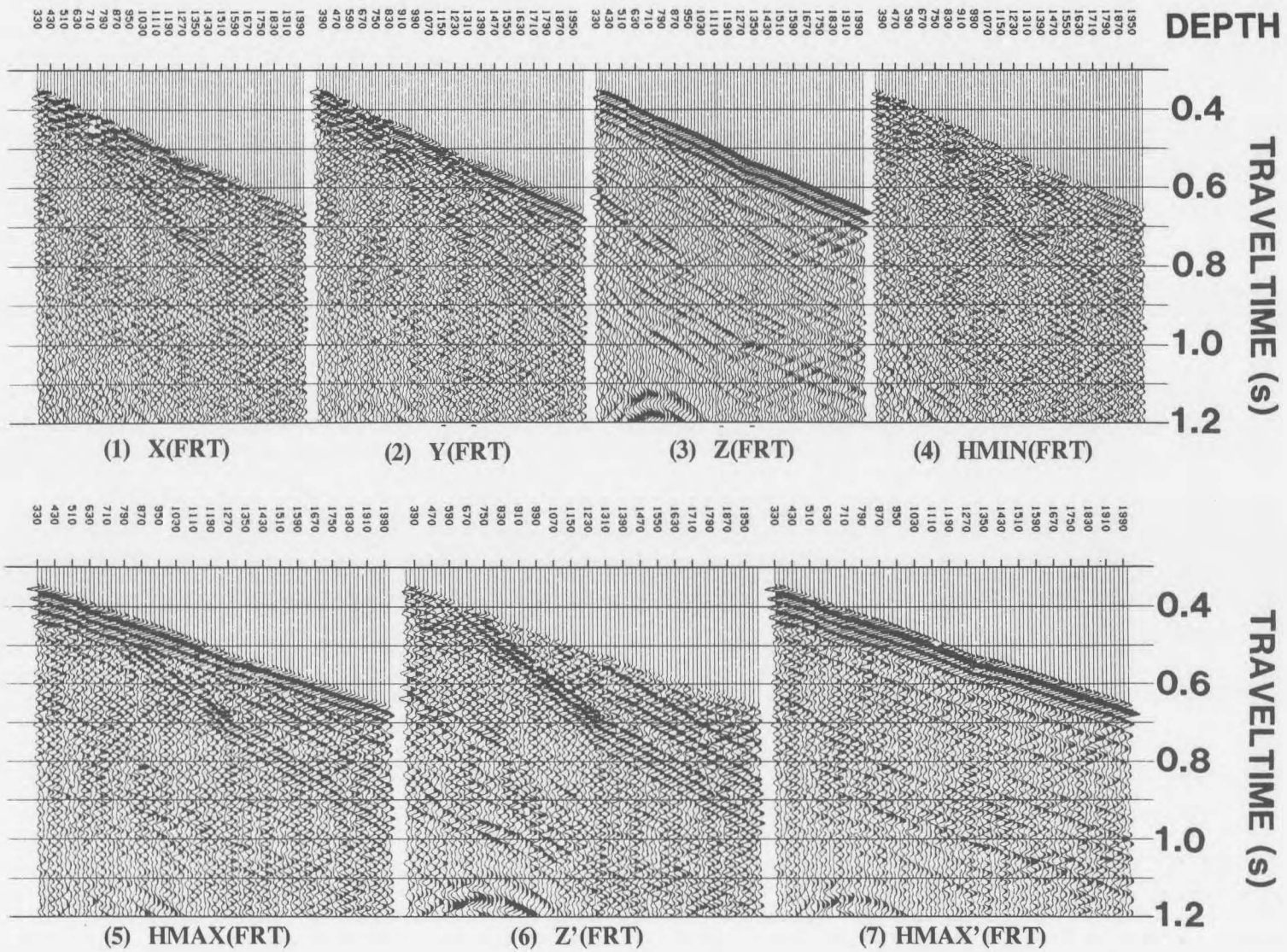

Figure 2.45 Hodogram-based polarization IPP for the Fort St. John Graben (FSJG2) far offset data (Hinds et al., 1993a). The downgoing P-wave events have been isolated on the **HMAX'(FRT)** data in panel (7).

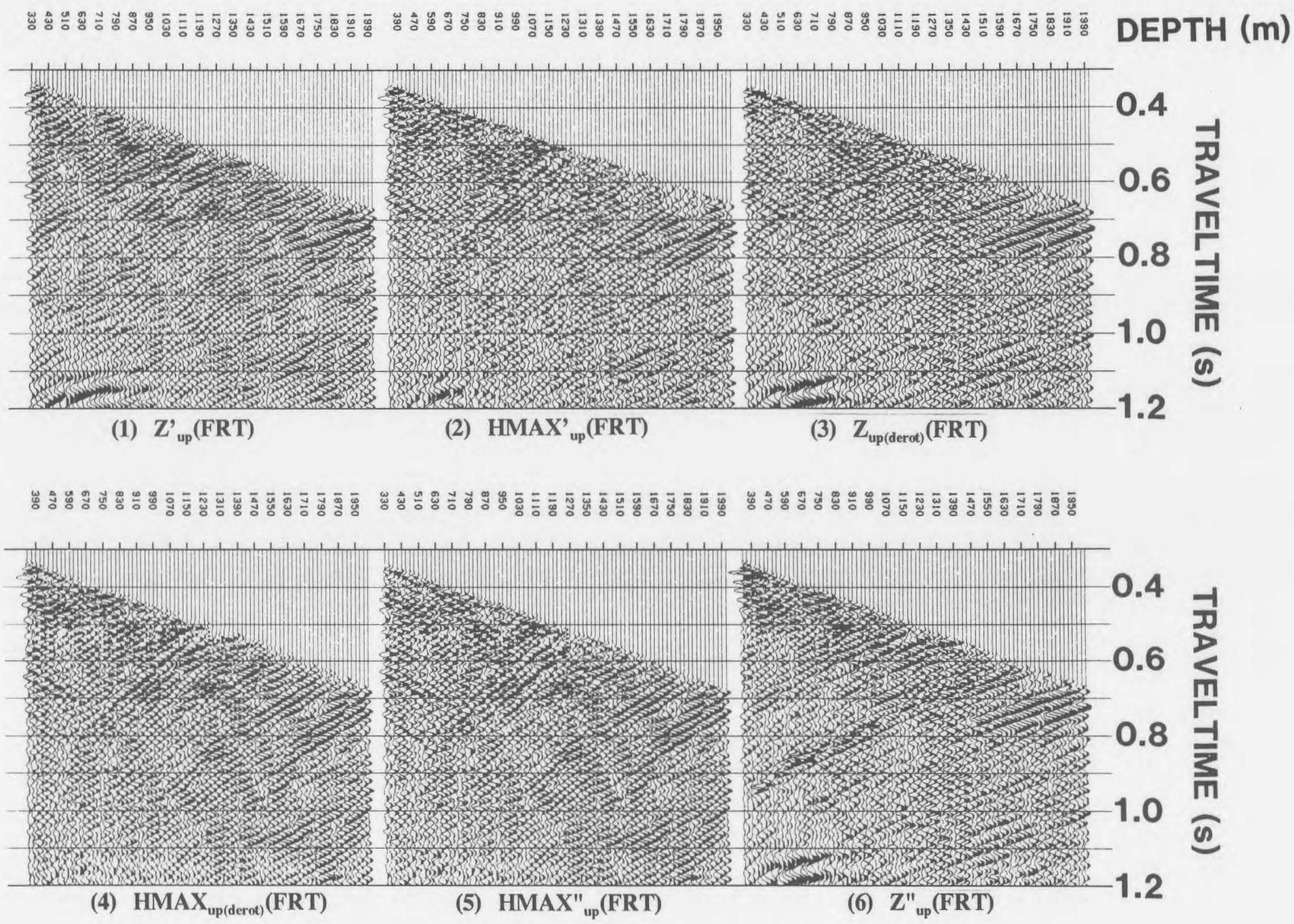

Figure 2.46 Time-variant polarization IPP for the Fort St. John Graben (FSJG2) far offset data (Hinds et al., 1993a). The upgoing P-wave events have been predominately partitioned onto the **Z"$_{up}$(FRT)** panel.

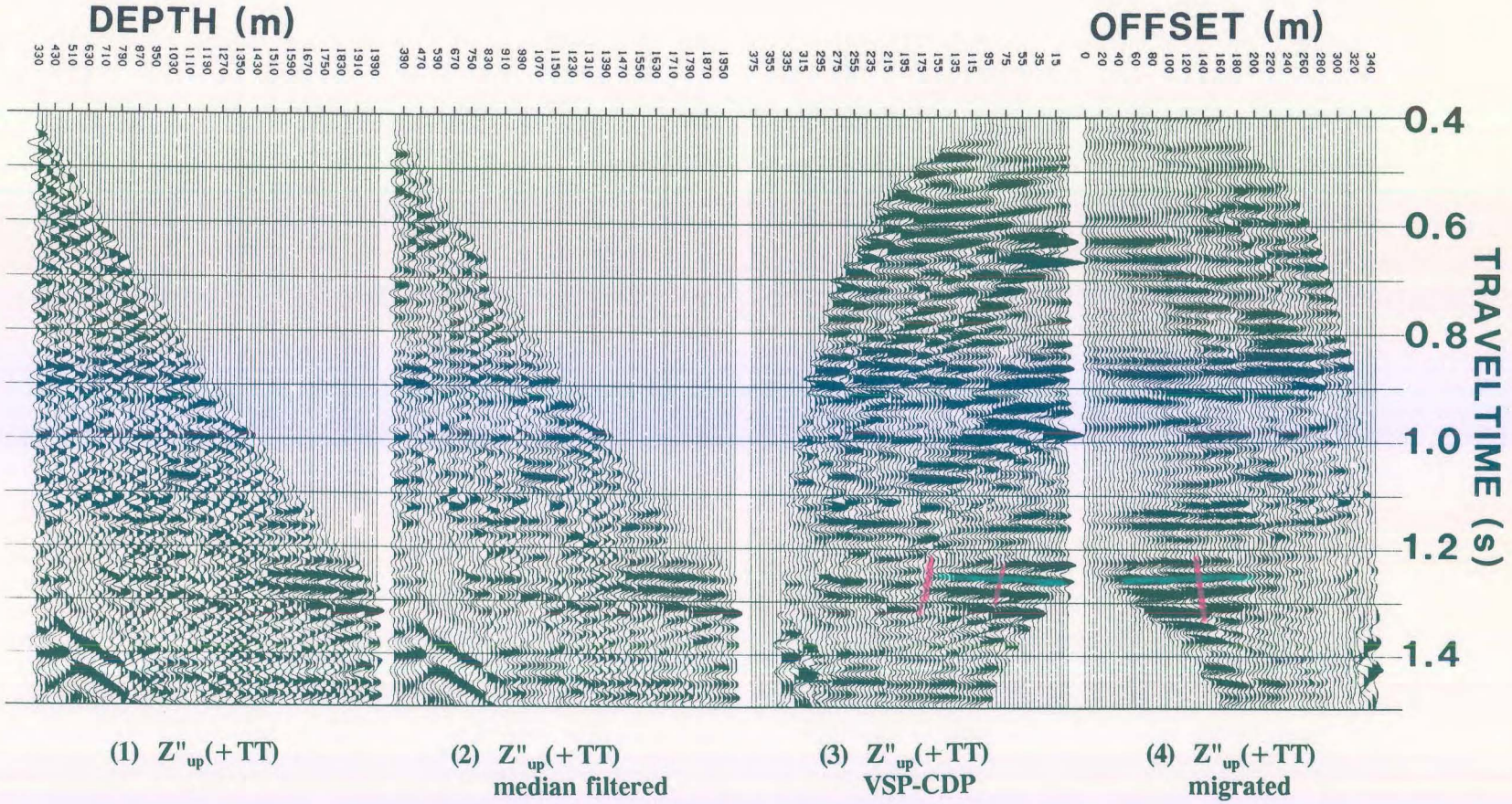

Figure 2.47 VSP-CDP and Kirchhoff migration IPP for the Fort St. John Graben FSJG2 far offset data (Hinds et al.,1993a). Note the continuity of the event (peak) on the VSP-CDP display at 1.27 s (from offset traces 0-55 m).

The VSP (far offset) deconvolution has not received attention in the literature because the decision to deconvolve the far offset is usually made after interpretation. Whereas, deconvolution of near offset VSP data would be done as a matter of course, the far offset deconvolution decision-making would follow the course of:

(1) searching for possible interfering multiples on the far offset $\mathbf{Z"_{up}(+TT)}$;

(2) confirming that the event is not a terminating reflector located away from the borehole;

(3) utilization of the $\mathbf{Z'_{down}(-TT)}$ data to deconvolve the $\mathbf{Z"_{up}(+TT)}$; and

(4) reconfirming the interpretation by comparing the data before and after deconvolution.

This illustrates the arduous task presented to the "interpreter/processor".

The VSP-CDP/migration IPP for the far offset data of the Simonette carbonate reef case study (Chapter 6; Hinds et al., 1991b; Hinds et al., 1993b and 1994c) is presented in Figure 2.48. The data contain destructively interfering multiples (coloured green). On panel 2, the off-reef carbonate (coloured "reef" purple; see chapter 6 or Hinds et al., 1993b and 1994c) starts at 1.96 s on the deepest trace and climbs onto the low-relief reef mid-way across the display rising up onto the peak event at 1.92 s (the transition being between depth levels 2470 - 2570 m).

There is an anomalous event (peak) at 1.8 s that does not seem to correspond to the geology interpreted from the sonic log. The Wabamun Formation (highlighted in red; see Chapter 6) event intersects the first break curve at 3020 m as a peak at 1.735 s in the $\mathbf{Z"_{up}(+TT)}$ data. Note that the anomalous event (the peak colored green for reference) between 1.77 - 1.81 s lies immediately under the Wabamun event and does not intersect the first break

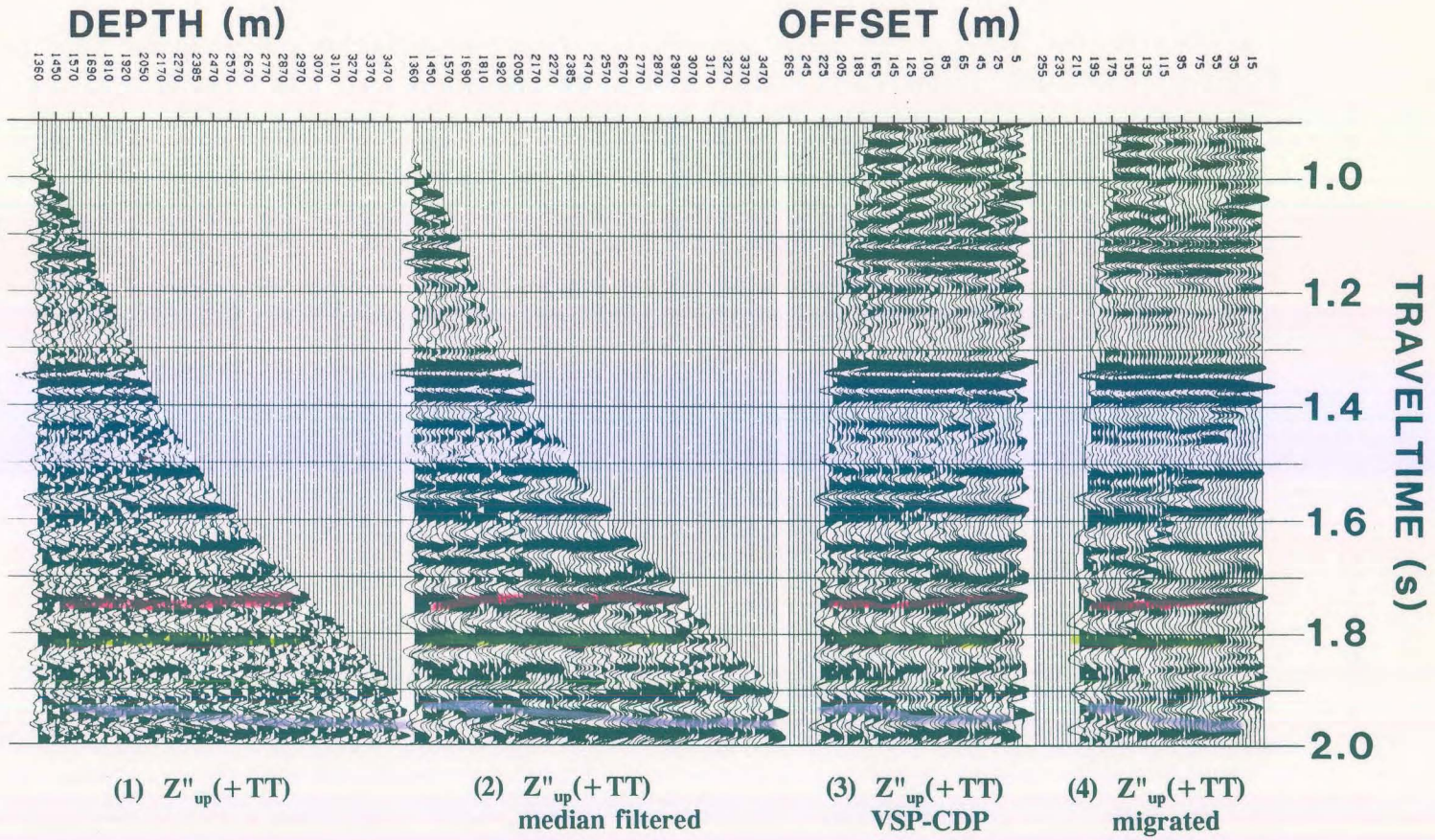

Figure 2.48 VSP-CDP and migration IPP for the Simonette far-offset non-deconvolved data (Hinds et al., 1993b). A possible multiple event occurs at 1.8 s (peak).

curve. This may be a real geological event that phases out before the borehole and subsequently would not be on the borehole logs; however, it could also be a multiple of the Wabamun primary event.

The $\mathbf{Z'_{down}(-TT)}$ data were used to deconvolve the $\mathbf{Z_{up}(+TT)}$ data from panel 1 of Figure 2.48 to output the $\mathbf{Z_{up(decon)}(+TT)}$ data in panels 1 and 2 of Figure 2.49. The deconvolution has been successful in attenuating the possible multiple and the interpretation of the reef events (in "reef" purple) can proceed on the VSP-CDP and migrated data shown in panels 3 and 4. The two IPP's shown in Figure 2.48 and 2.49 can be interpreted cooperatively in order to interpret through possible deconvolution noise.

2.3.5. Problematic far offset interpretive processing

In this section, the far offset polarization and deconvolution processing of the Ricinus carbonate reef case study (Hinds et al., 1989a; Hinds et al., 1993c; Hinds et al., 1994c) shall be presented. The case study presented in Chapter 4 also highlights the difficulties within the data processing that were solved through the interpretive processing of the far offset data; however, in the context of more detailed interpretation.

The two procedures that will be shown are:

(1) the far offset time variant polarization; and

(2) far offset deconvolution.

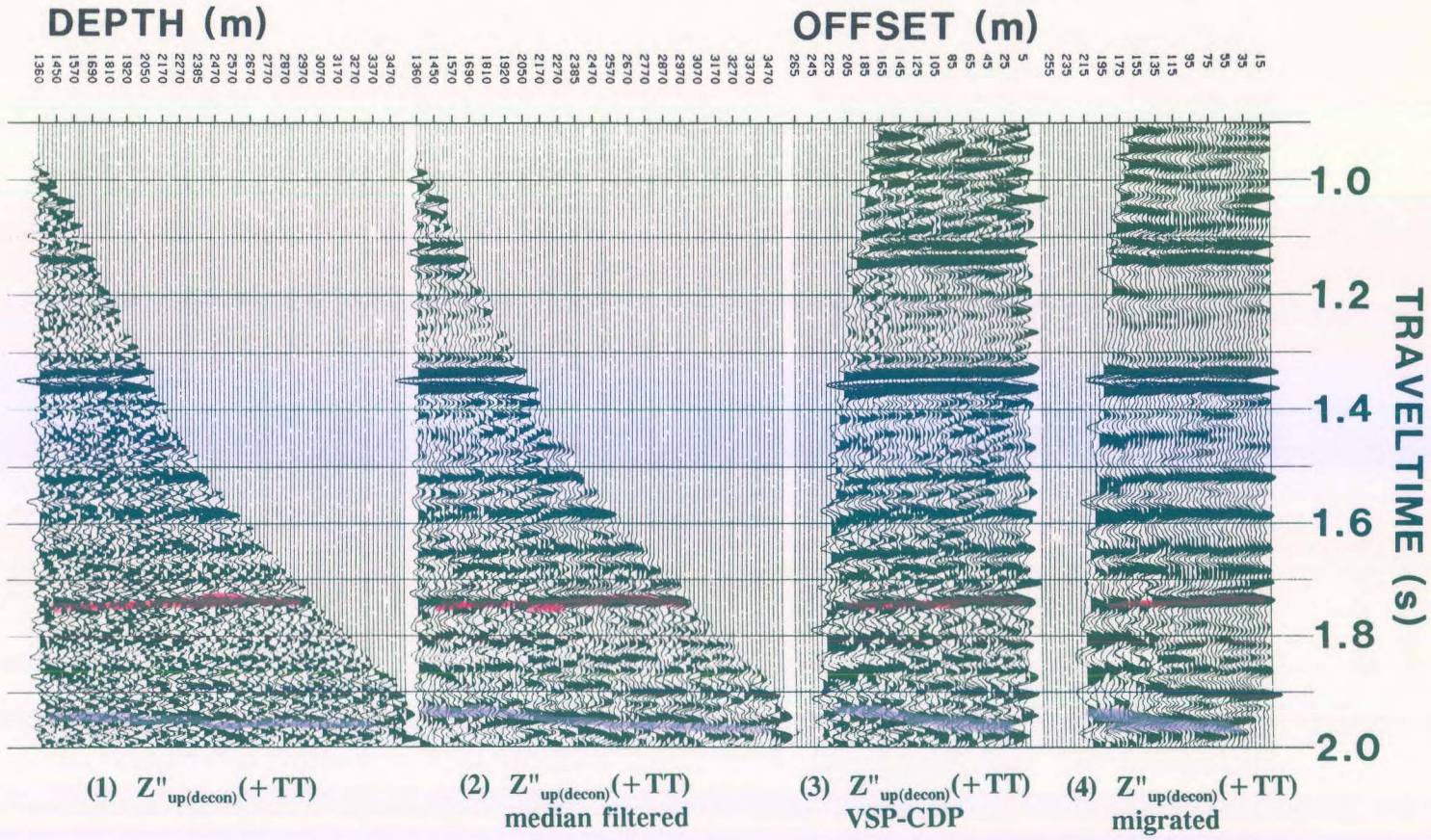

Figure 2.49 VSP-CDP and Kirchhoff migration IPP for the Simonette far-offset deconvolved data (Hinds et al., 1993b). The suspected multiple at 1.8 s has been attenuated; however, the reef interpretation (detailed in chapter 6) remains.

2.3.5.1 Time variant polarization of the Ricinus case study data

Figure 2.50 shows the time variant polarization IPP for the Ricinus carbonate reef case study (Chapter 4) far-offset (1100 m) data after "normal" processing. The processing followed the guideline far offset processing runstream presented in section 2.1.

The **Z"$_{up}$(FRT)** data (panel 6) is contaminated with diffractions and mode-converted SV up- and downgoing events highlighted in yellow. The same mode-converted SV events, also highlighted in yellow, are shown in panel 1 of the VSP-CDP IPP in Figure 2.51. On panel 1 (Fig. 2.51), upgoing P events highlighted in orange intersect the first break "curve" between the 3300 and 3510 m traces. Linear events, highlighted in yellow, trending from the left hand bottom corner of panel 1 cross the data and merge with the highlighted (in orange) P-wave events. The yellow highlighted events represent the upgoing SV events that are contaminating some of the underlying P-wave data.

The downgoing mode-converted SV events can be seen better on panels 2, 3, 5 and 6 of Figure 2.50. These linear events (highlighted in green) trend in the same direction as the P-wave first break "curve" but at a steeper dip (implying a slower apparent velocity).

The first break "curve" does not exist following the downgoing wavefield separation processing. The "curve" refers to the mute limit on the data chosen using the first breaks.

The second stage of interpretive processing is now accomplished. By interpreting the "noise" (mode converted up- and downgoing SV events), the interpreter/processor can begin to

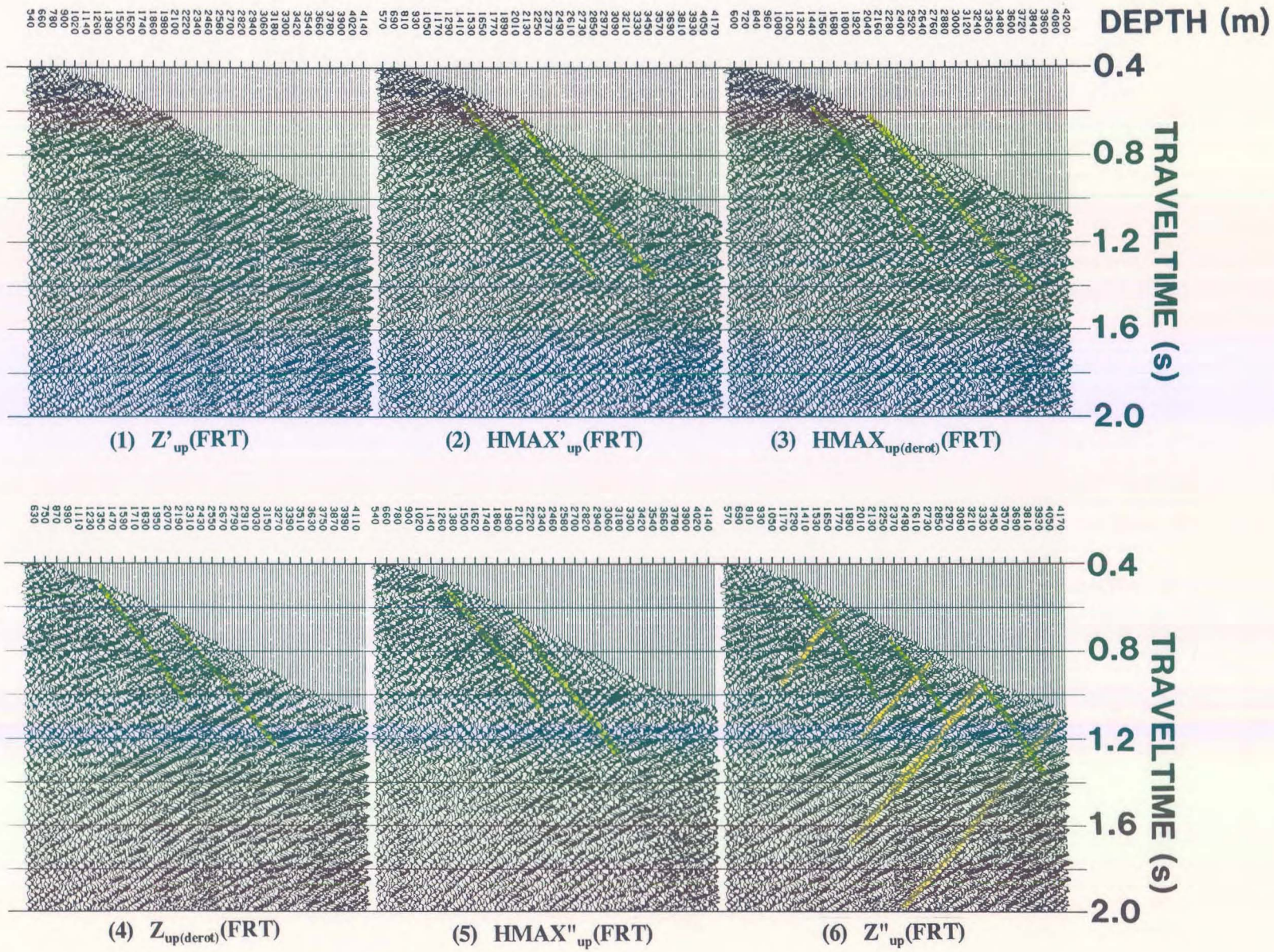

Figure 2.50 Time-variant polarization IPP for the Ricinus data (Hinds et al., 1989a; Hinds et al., 1994b) using the example far-offset processing initially presented in the "processing runstreams" section of chapter 2.

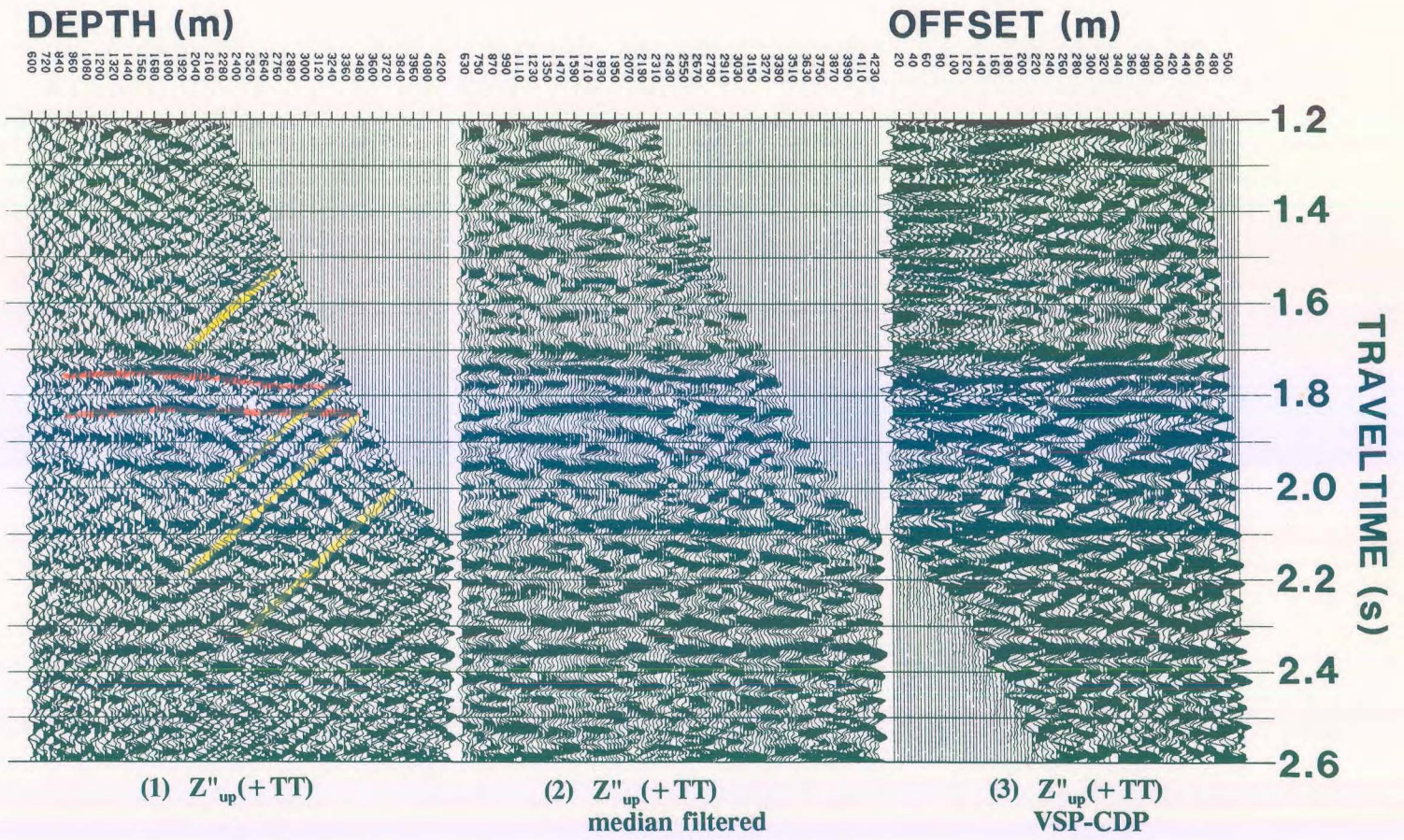

Figure 2.51 VSP-CDP IPP for the Ricinus data (Hinds et al., 1989a; Hinds et al., 1993c) using the $\mathbf{Z}''_{up}$ data shown in Figure 2.50. The upgoing P-wave events are difficult to interpret due to up- and downgoing SV-wave events.

redesign the processing to minimize the "unwanted" noise.

It was decided to go back to the **Z(FRT)** and **HMAX(FRT)** data and perform the wavefield separation on these two data panels (and not the **Z'(FRT)** and **HMAX'(FRT)** data as suggested in the processing guidelines of section 1.2). The wavefield separation processing included the attenuation of the mode-converted SV events. The results of the new processing runstream are shown in the updated time variant IPP shown in Figure 2.52.

The input **HMAX(FRT)** and **Z(FRT)** data are shown in panels 1 and 2. The wavefield separated $\mathbf{HMAX_{up}(FRT)}$ and $\mathbf{Z_{up}(FRT)}$ data in panels 3 and 4 can now be compared to the original $\mathbf{HMAX_{up(derot)}(FRT)}$ and $\mathbf{Z_{up(derot)}(FRT)}$ data in panels 3 and 4 of Figure 2.50 (the guideline runstream processing). Bypassing the (**Z**, **HMAX**) to (**Z'**, **HMAX'**) rotation (and possible noise generation caused by the polarization), the upgoing P events (some are highlighted in orange in panels 3 and 4 in Fig. 2.52) are more interpretable on the new processing. Time-variant polarization of the $\mathbf{HMAX_{up}(FRT)}$ and $\mathbf{Z_{up}(FRT)}$ data produces the $\mathbf{HMAX"_{up}(FRT)}$ and $\mathbf{Z"_{up}(FRT)}$ data shown in panels 5 and 6.

The VSP-CDP IPP display shown in Figure 2.53 for the modified processing runstream shows that the upgoing P events are much easier to follow and subsequently to interpret than the results presented in the VSP-CDP IPP using the original processing (Fig. 2.51). An example of this are the upgoing events highlighted in orange on panels 1 of Figures 2.51 and 2.53.

The $\mathbf{Z"_{up(med)}(+TT)}$ data in panel 2 of Figure 2.53 was created using a 5 point median filter

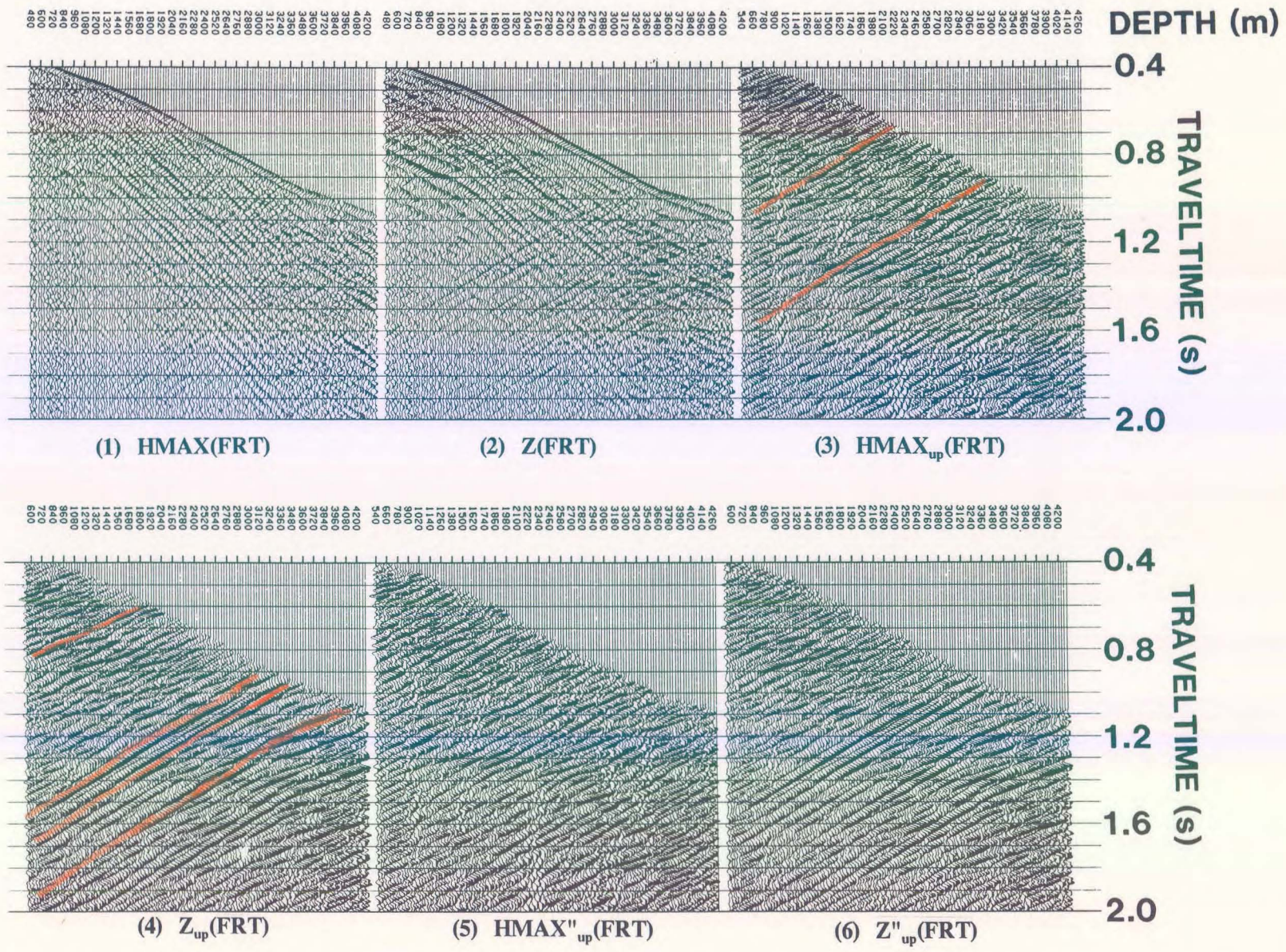

Figure 2.52 Modified time-variant polarization and wavefield separation IPP for the Ricinus data (Hinds et al., 1993c) following processing decisions made using interpretive processing.

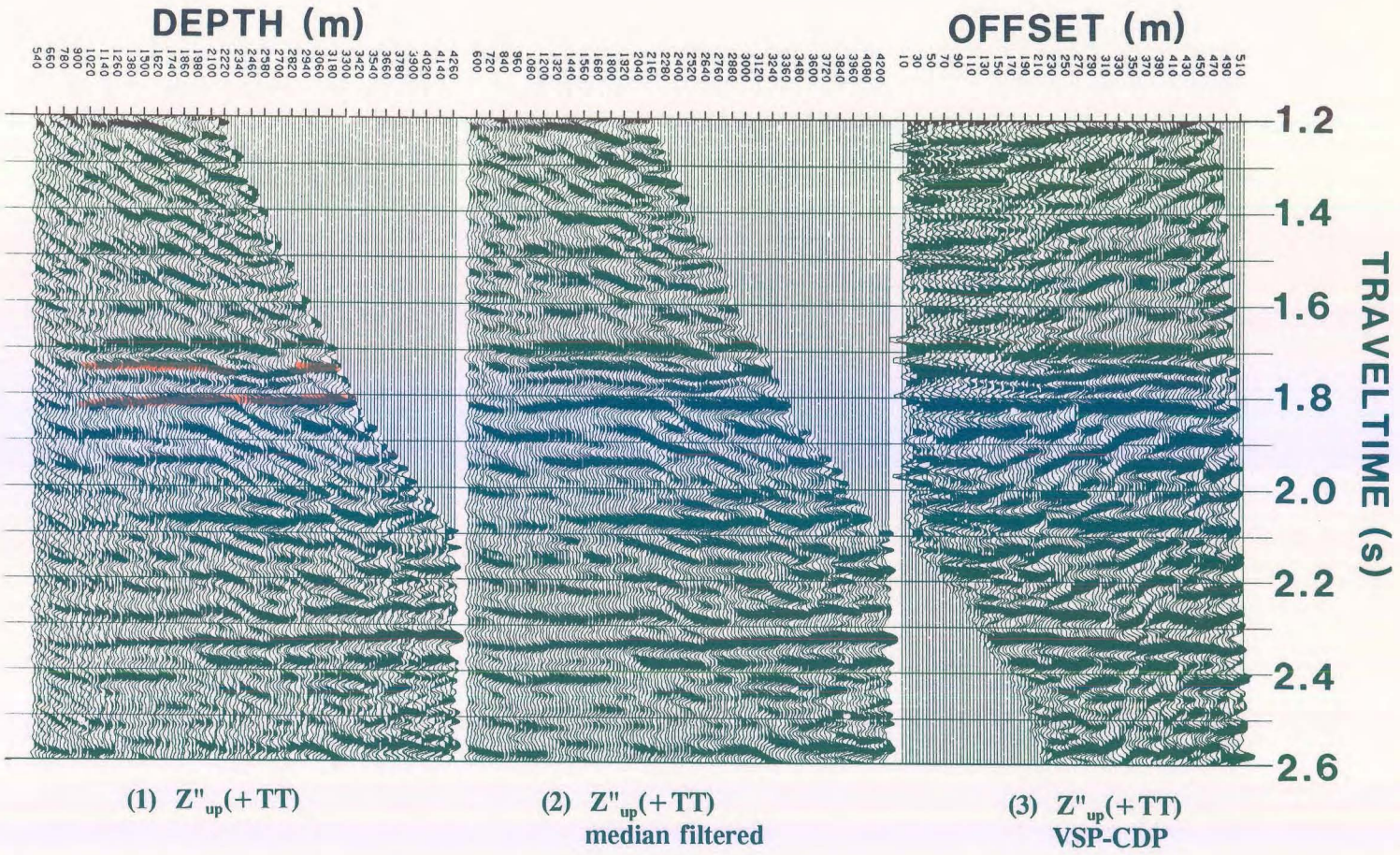

Figure 2.53 VSP-CDP IPP for the Ricinus data (Hinds et al., 1989a; Hinds et al., 1994b) using the $\mathbf{Z''_{up}}$ data shown in Figure 2.52. The upgoing P-wave events are more interpretable although the diffraction and downgoing SV-wave events have not been completely eliminated.

on the data seen in panel 1. Additional VSP-CDP displays using 9 and 11 point median filters to enhance the upgoing events on the **Z"$_{up}$(+TT)** data are shown in Figures 2.54 and 2.55, respectively. As noted before, the interpreter/processor would derive an interpretation from Figures 2.53 to 2.55; however, one would also verify that the same events are resident on Figure 2.51. Interpretive processing includes every piece of information available during the interpretation stage.

2.3.5.1 Far offset deconvolution of the Ricinus case study data

In this section, the far offset deconvolution of the Ricinus carbonate reef case study (Hinds et al., 1989a; Hinds et al., 1994c) is examined. The deconvolved far offset results are also presented in Chapter 4 (Hinds et al., 1994c) in order to examine the evaluation of deconvolution generated noise testing in the context of a case study.

The far offset deconvolution IPP for the Ricinus far offset (1100 m) data is shown in Figure 2.56. The **HMAX'(-TT)** and **HMAX'$_{down}$(-TT)** data are shown in panel 1 and 2, respectively. By inspection, the **HMAX'$_{down}$(FRT)** data do not posses an abundance of multiple events. Few, if any, multiple events are seen after the primary downgoing event.

The deconvolution verification panel contains the deconvolved downgoing events and is shown in panel 3. This is the result of applying the deconvolution processing to the downgoing events themselves. The **Z"$_{up}$(-TT)** data of the updated interpretive processing

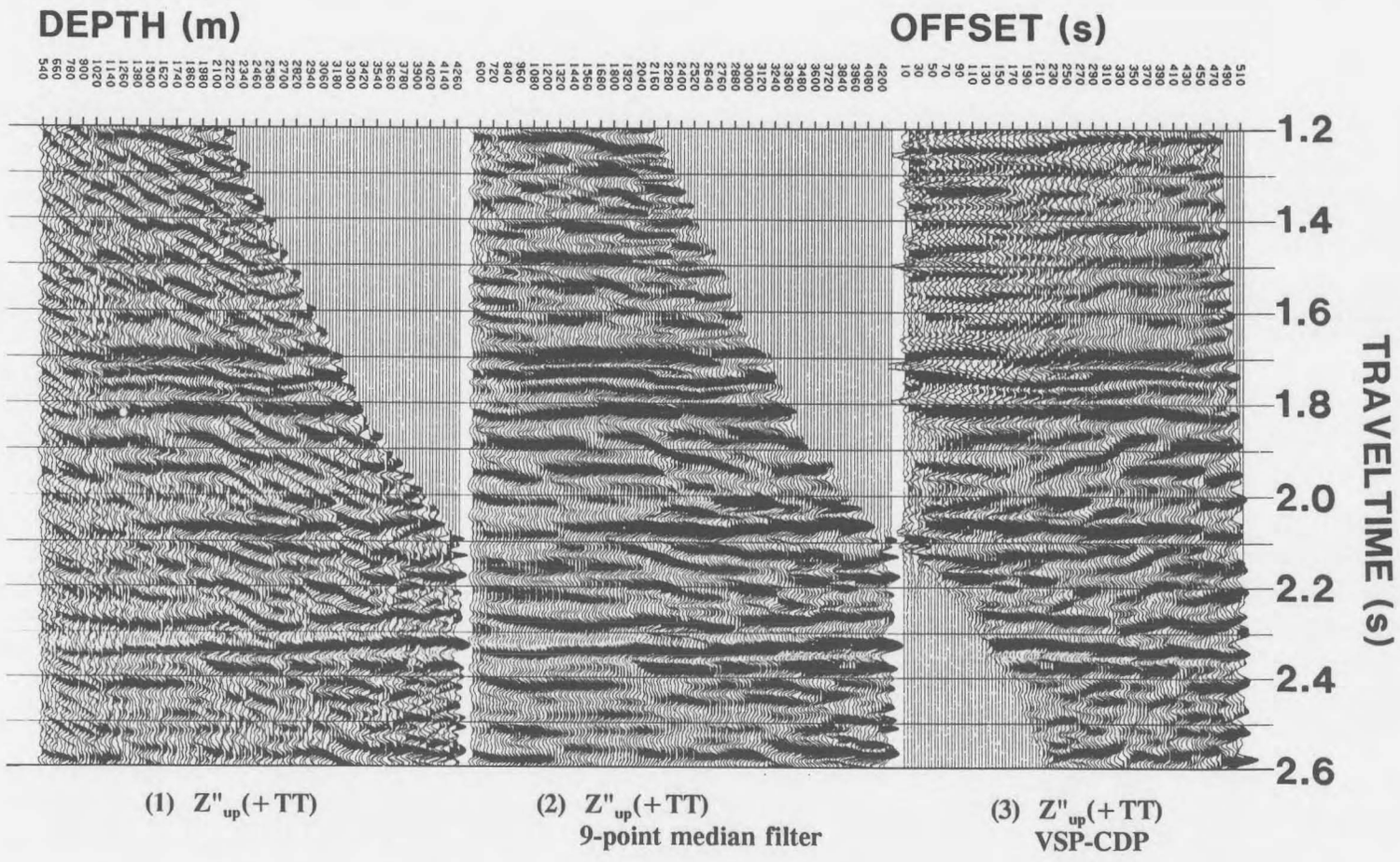

Figure 2.54 VSP-CDP IPP for the Ricinus data (Hinds et al., 1994b) with the Z''_{up} data shown in Figure 2.51 as input and data enhancement using a 9-point median filter.

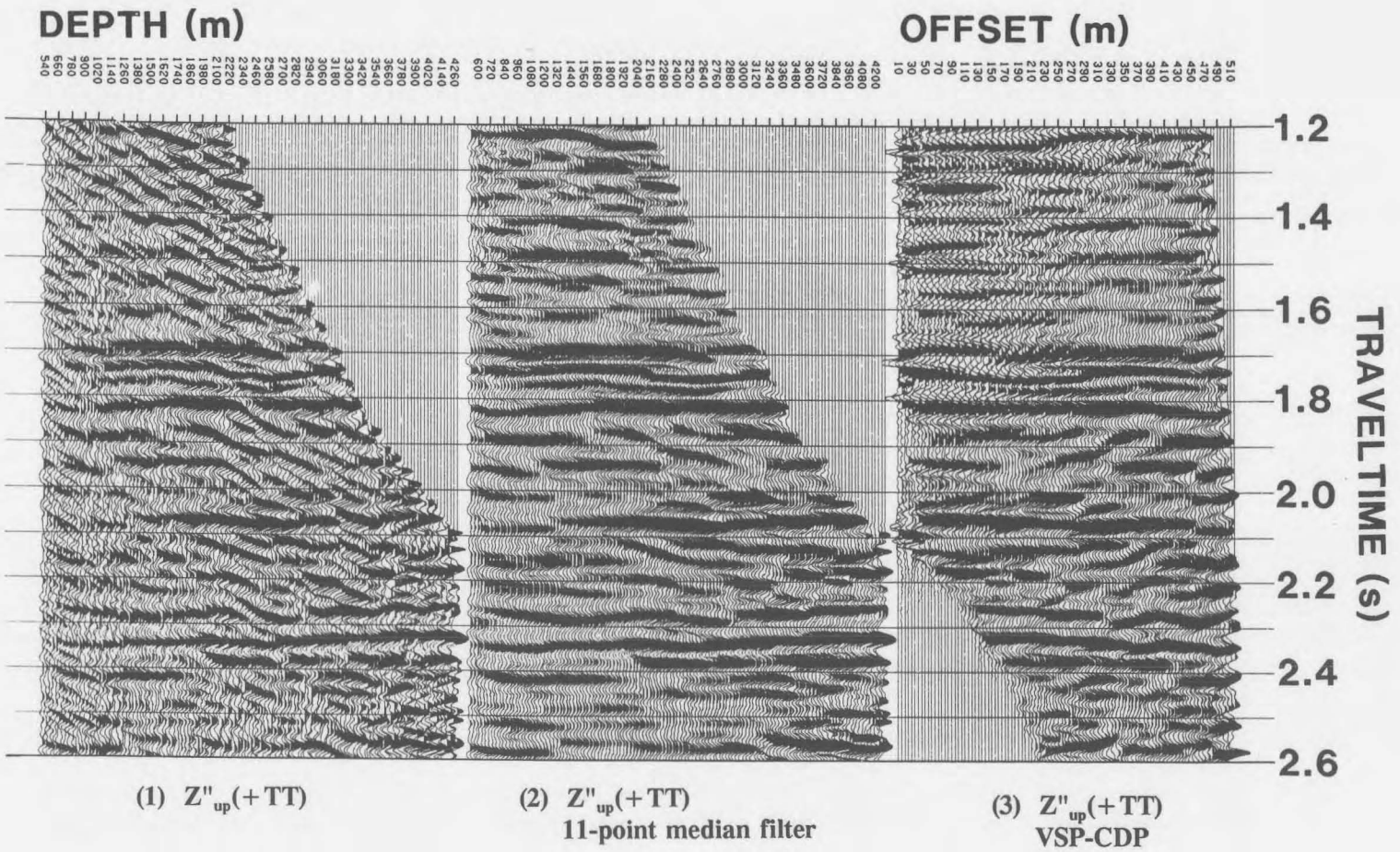

Figure 2.55 VSP-CDP IPP for the Ricinus data (Hinds et al., 1994b) with the Z''_{up} data shown in Figure 2.51 as input and data enhancement using a 11-point median filter.

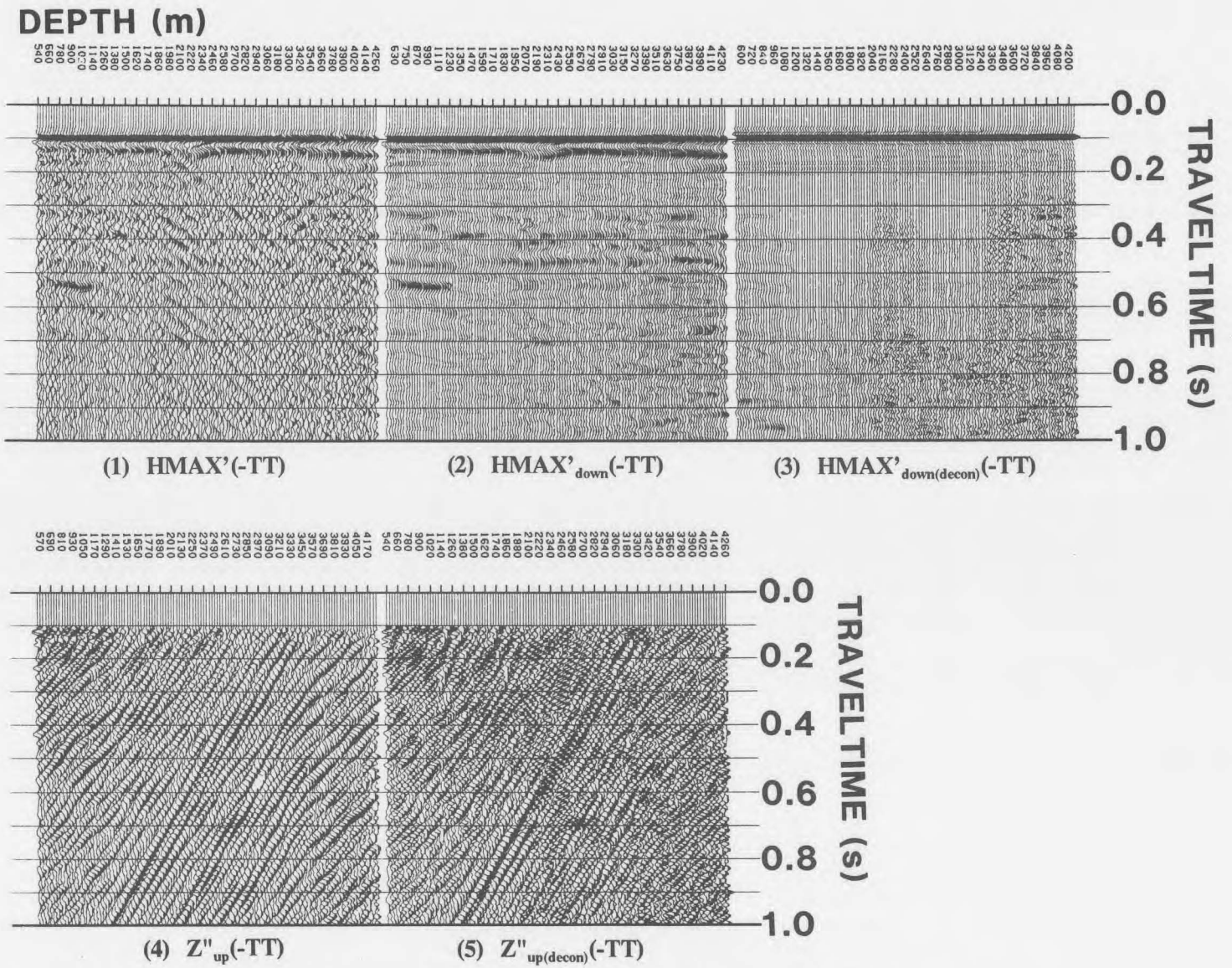

Figure 2.56 Far offset deconvolution IPP for the Ricinus data (Hinds et al., 1994b). Note the deconvolution induced noise by comparing panels 4 and 5.

(shown in Fig. 2.52) are shown in panel 4. The $\mathbf{Z''_{up(decon)}(-TT)}$ data are shown in panel 5. By inspection of panels 4 and 5, the deconvolution process has added undesirable noise to the upgoing event data.

The VSP-CDP IPP of the $\mathbf{Z''_{up(decon)}(+TT)}$ data is shown in Figure 2.57. The interpretation of the data was damaged by the addition of deconvolution noise. One reason for the deconvolution processing failure is that the simple time delay relationship between up- ($\mathbf{Z''_{up}}$) and downgoing ($\mathbf{HMAX'_{down}}$) events may not be satisfied for the far-offset data (1100 m offset).

2.4 Integrated displays

2.4.1 Integrated Log Display (ILD)

The integrated well log display highlights the seismic data around the well, the geological log data (in time) and the synthetic seismogram as shown in Figure 2.58. This display is included because, in practice, the VSP survey is usually the final survey to be run on a well following the acquisition of the geological logs. By the time that the VSP is processed, the sonic log should have been digitized and ready for the "check-shot" type of calibration.

Whilst the VSP is being processed, the near offset VSP first break times can be used to calibrate the sonic log (correct for sonic log drift and tie the integrated sonic log to the VSP first break times). The seismogram and calibrated sonic log (merged onto the seismic line

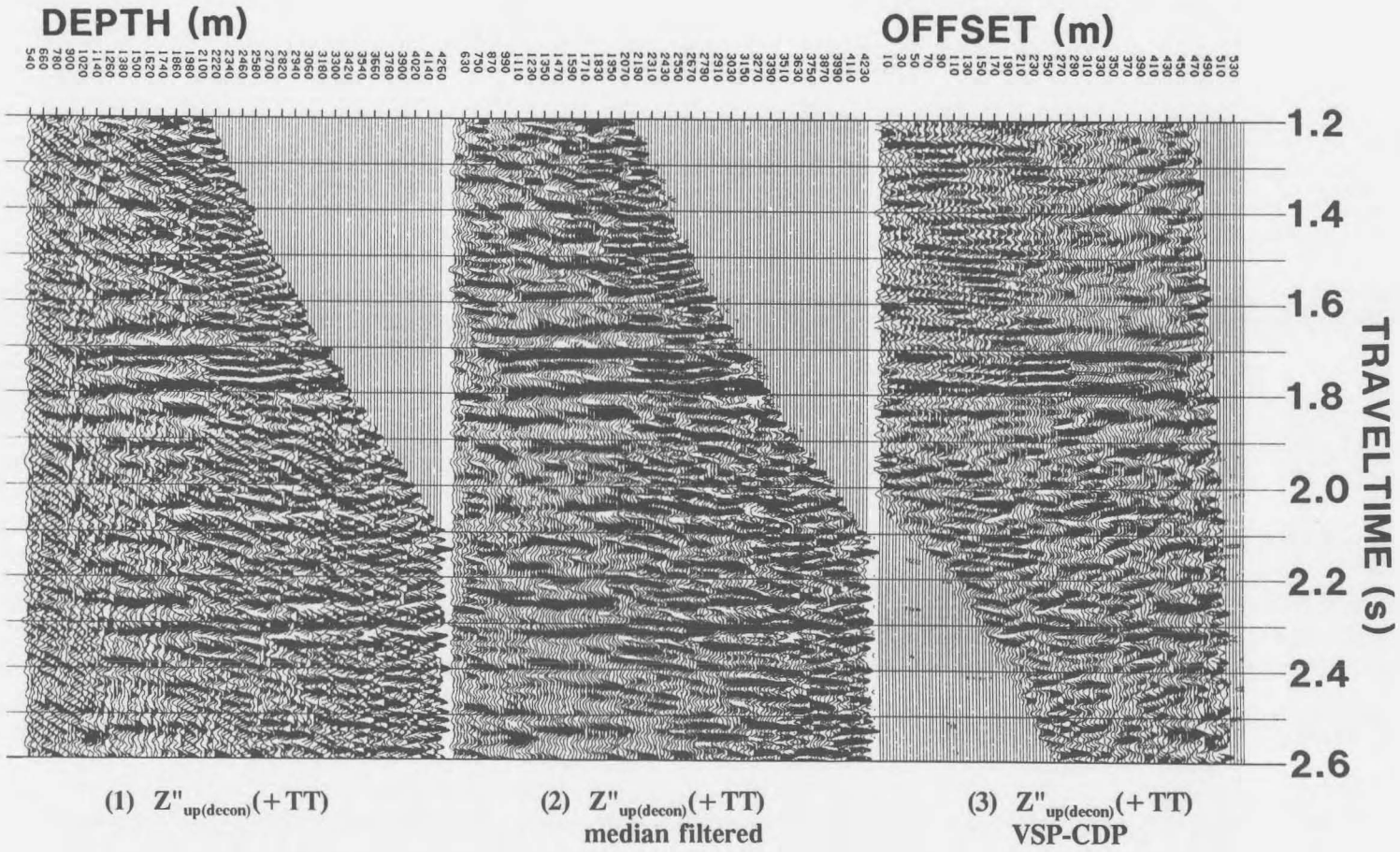

Figure 2.57 VSP-CDP IPP for the Ricinus $Z''_{up(decon)}(+TT)$ data (Hinds et al., 1994b). The deconvolution was not successful and was dropped from the Ricinus case study "normal" far offset processing runstream flow.

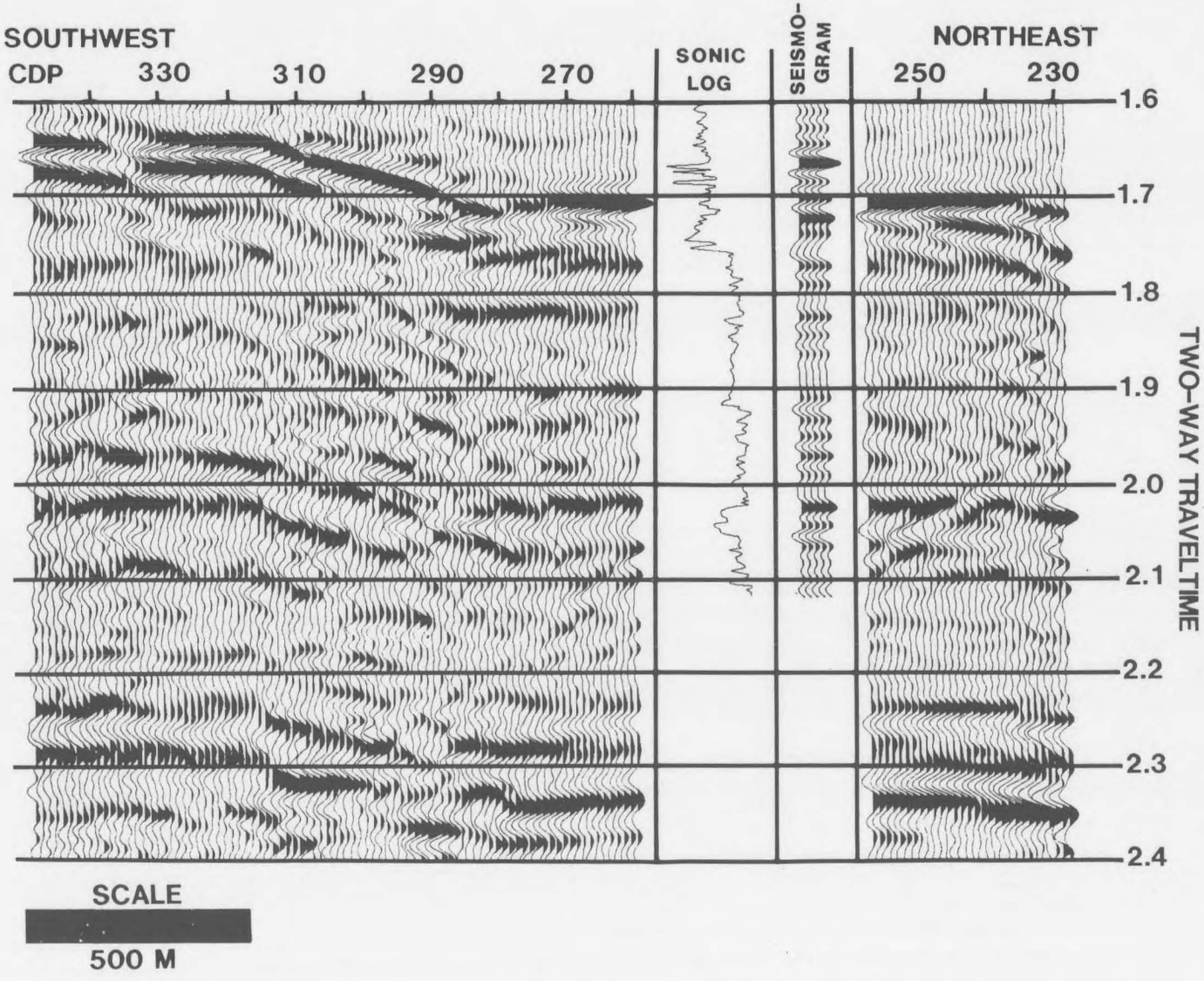

Figure 2.58 Integrated log display (ILD) for the Ricinus data (Hinds et al., 1989a; Hinds et al., 1994b).

on the ILD) can assist the interpreter to get a first-hand look at the location of the seismic events that were "intersected" by drilling.

2.4.2 Integrated Seismic Display (ISD)

The integrated seismic display for the Ricinus carbonate reef case study (Hinds et al., 1989a; Hinds et al., 1993c; Hinds et al., 1994c) is shown in Figure 2.59. The display contains the VSP-CDP (or migration) results merged with the surface seismic. The VSP-CDP is lateral offset data imaging the reflectors away from the well and can provide a high-resolution image of the reflectors in comparison to the same events seen on surface seismic.

2.4.3 Integrated Interpretive Display (IID)

At the final presentation stage of the project, a large part of the geoscience exploration results should be displayed. This is accomplished using the integrated interpretive display. The IID shown in Figure 2.60 displays the integrated results from the Simonette carbonate reef case history (Hinds et al., 1991b; Hinds et al., 1993b and 1994c).

This case study involves using the data to substantiate the need for a well "whipstock". It

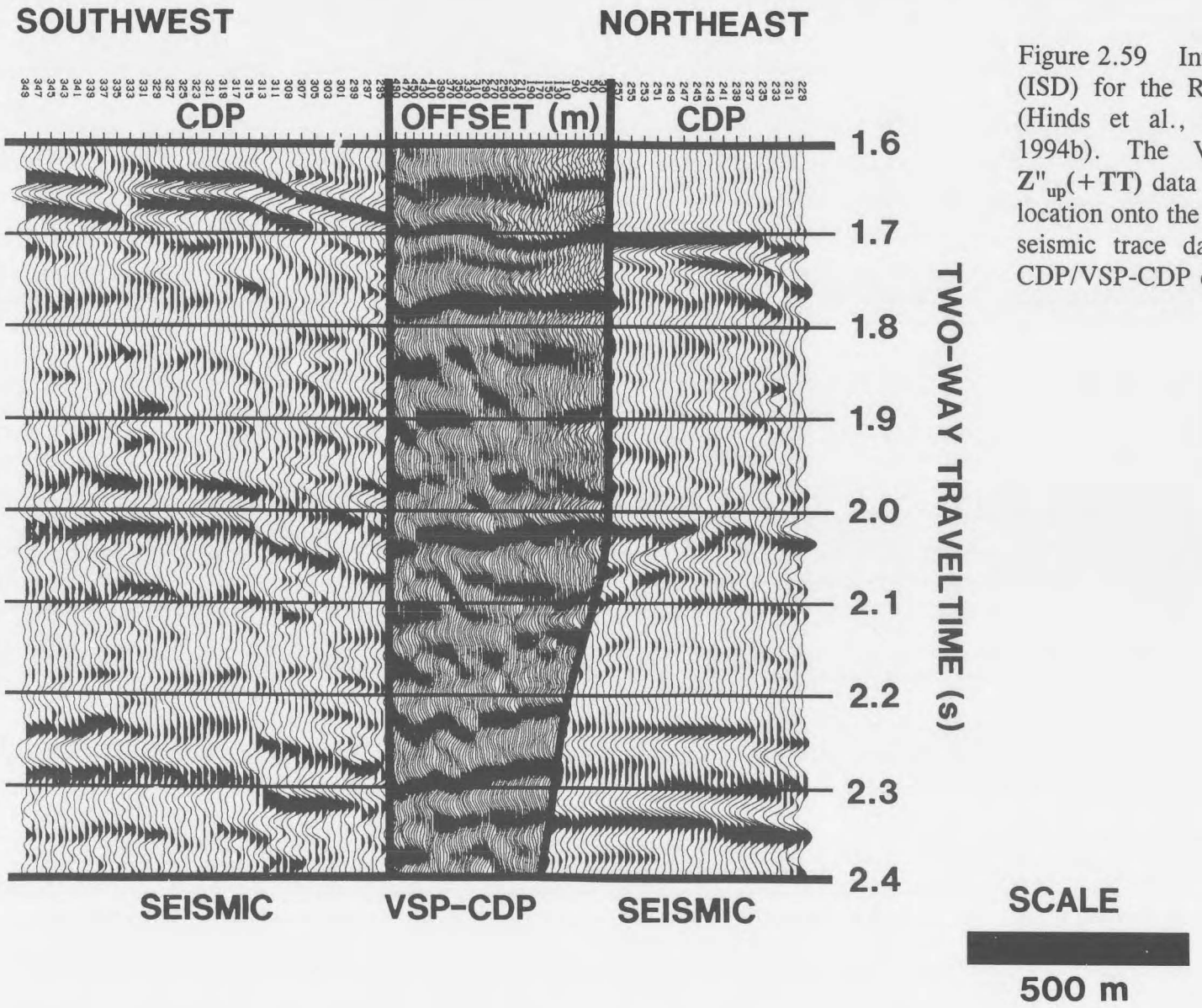

Figure 2.59 Integrated seismic display (ISD) for the Ricinus case study data (Hinds et al., 1989a; Hinds et al., 1994b). The VSP-CDP transformed $Z''_{up}(+TT)$ data are inserted at the well location onto the seismic and replace the seismic trace data at the overlapping CDP/VSP-CDP offset locations.

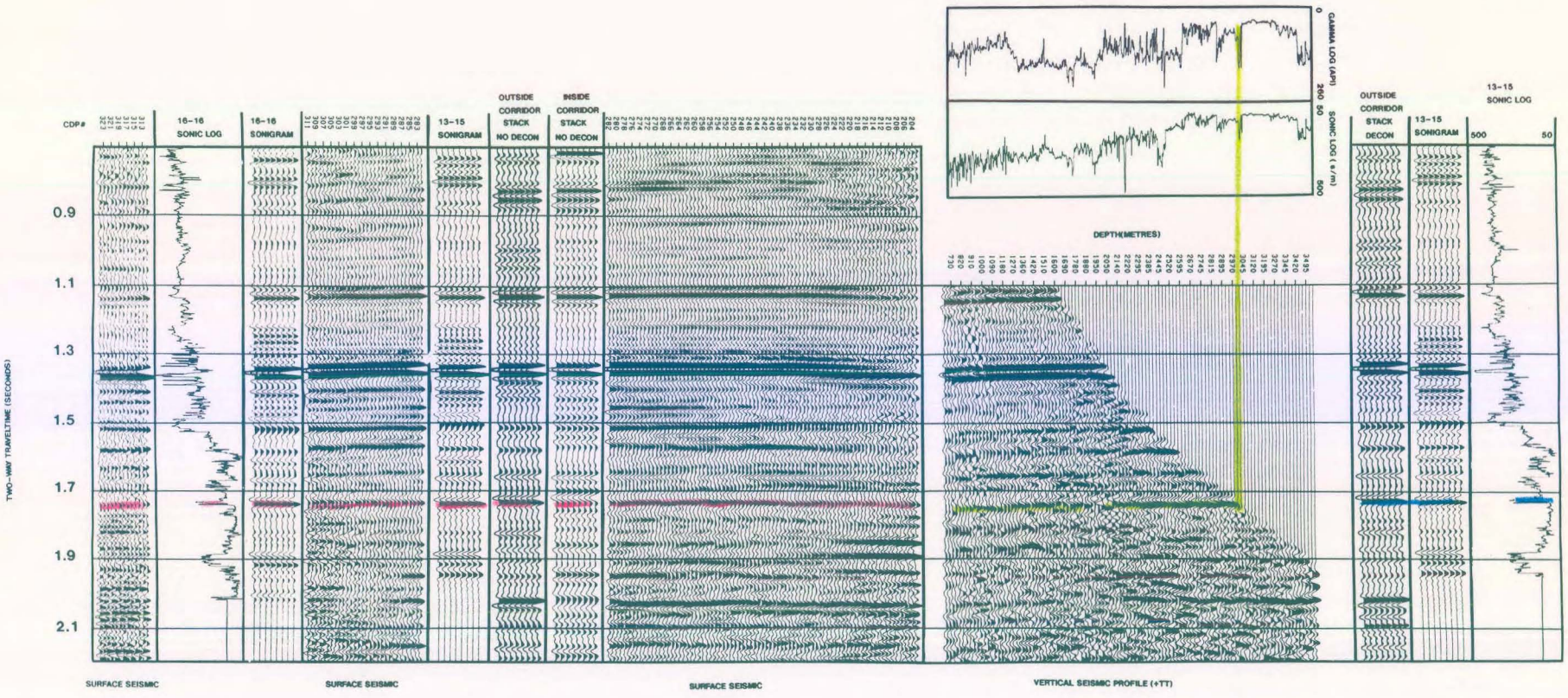

Figure 2.60 Integrated Interpretive Display (IID) of the Lanaway case study data (Hinds et al., 1989a; Hinds et al., 1994a). The display includes sonic and gamma logs (both in time and depth), the $\mathbf{Z_{up}(+TT)}$ VSP data, corridor stack results and surface seismic data. This panel incorporates all of the exploration data for the area onto one single display for easy integrated interpretation.

was interpreted that the reef is beyond the "economic" reach of the whipstock (Hinds et al., 1993b and 1994c). The IID is used to conveniently show the lateral coverage and the interpretation away from the well towards the "known" reef on the far offset VSP in conjunction with the information available from the other types of exploration data.

The IID can be used to explain the entire interpretation procedure and how the different datasets tie. For example, the Wabamun Formation interface was interpreted from the sonic and gamma log to be at 3020 m well depth. Starting with the sonic and gamma logs in depth on Figure 2.60, a line can be drawn through the sonic and gamma high (at 3020 m) down to the upgoing (peak) event that intersects the 3020 m depth trace on the far offset $\mathbf{Z''_{up}(+TT)}$ data. This line is shown in green on Figure 2.60. The Wabamun seismic marker is now tied to the logs through the common depth axis of the far offset VSP data (centre panel) and the logs (located above the centre panel).

The Wabamun VSP event can be tied to the surface seismic event at the 13-15 well using the time tie from the geologic logs. To the right of the VSP data are the outside corridor stack after deconvolution (to show primary events), the 13-15 synthetic seismogram and the 13-15 sonic log displayed in two-way traveltime. Using the tie of the VSP to the geologic logs, an interpreted Wabamun event can be further confirmed by tying the event (on the 3020 m trace) to the corridor stack, sonigram and sonic log (in time). This is shown by a blue line in Figure 2.60.

This tie can be drawn on the 13-15 sonigram, outside corridor stack of the $\mathbf{Z_{up(decon)}(+TT)}$ data and inside corridor stack of the $\mathbf{Z_{up}(+TT)}$ data that are spliced into the surface seismic

at the 13-15 well location. This is seen on the left panel of Figure 2.60. The nondeconvolved inside corridor stack would enable an interpretation of multiples on the surface seismic at the 13-15 well location. The interpretation of the Wabamun event (shown in red) is extrapolated onto the surface seismic on either side of the well. The 16-16 sonic log (in time) and 16-16 sonigram are spliced into the seismic section at the 16-16 well location. This will enable the interpretation of the reef at the 16-16 location.

The interpreted basal reef marker rising onto the reef pinnacle can be shown on the far offset VSP data panel (see chapter 6 or Hinds et al., 1991b and 1993b; Hinds et al., 1994c).

The VSP-CDP IPP displays would complete the presentation (Figs. 2.48 and 2.49) by showing the reef interpretation at the well and laterally offset for 200 m away from the well towards the "known" reef (at the 16-16 well). Questions about the effects of multiples are answered and the tie of the geology to the geophysics is resolved. The economics are discussed in the view of production penalties (caused by whipstocking the well onto another company's "zone") and the interpretation that the reef is encountered approximately 120 m away from the new well.

Interpretive processing has driven the processing and the various IPP and displays confirm the interpretation.